Speeds of sound in a biogas mixture CH_4+N_2+CO_2+CO from T = [273,325] K and p = [1,12] MPa measured with a spherical resonator

Submitted by: Daniel Lozano Martín
Directed by: José Juan Segovia Puras

Abstract:

The present work has the objective of measure the speeds of sound in a biogas mixture of CH_4+N_2+CO_2+CO, in the pressure range p = [1,12] MPa and temperature range T = [273,325] K, by a spherical acoustical resonator. The results are fitted to the virial acoustic equation of state, obtaining the virial acoustic coefficients, β_a y γ_a, and they are extrapolated to null pressure, determining the adiabatic coefficient as perfect gas, γ^{pg}, and the isobaric and isochoric heat capacities as perfect gas, C_p^{pg} y C_V^{pg}, respectively. The speeds of sound are acquired with a maximum relative uncertainty of $350ppm$ and they are compared with the results predicted by the reference equation of state for methane mixtures (natural gas-like mixtures), the EoS GERG-2008: relative deviations between experimental data and values estimated by this model were lower than 700 ppm at T=325K, below 400 ppm and within the uncertainty of measurement at T=300K, but appreciably higher at isotherm T=273K at the highest pressure range of this work.

Keywords:

Speed of sound, acoustic resonance, spherical resonator, virial acoustic coefficients, heat capacities as perfect gas, biogas.

1. Introduction.

Under the development framework of energy sources to replace conventional fossil fuels, aim to make them cheaper, to emit lower amounts of CO_2 into the atmosphere and to supply the depletion of resources such as oil and coal at long-term, in the past decades natural gas-like mixtures, as biogas, have been arise as a possible alternative [1]. In order to continue contributing to its implementation, it is necessary to improve the thermodynamic models used for the calculation and design of the extraction, transportation, storage and distribution systems of biogas-like mixtures. Therefore, the motivation for this research focuses on discussing the scope of the accuracy of the standard equation of state, EoS GERG-2008, compared with measurements of the speed of sound through a biogas sample and with the thermodynamic properties (heat capacities) derived from these data; as well as provide new accurate experimental results so that, if the scientific community consider appropriate, it can be made new correlations to improve the model.

It is chosen to study a quaternary CH_4+N_2+CO_2+CO mixture synthesized in the laboratory, with the composition indicated in Table 1, instead of a gas sample obtained by natural a process of biodegradation of biomass with the goal to have a precise composition without impurities

unquantified to achieve the lowest possible measurement uncertainty. Works with others methane-like mixtures, binary in this case, have been previously reported by other authors: [2], [3], [4].

The spherical resonator (operating at low resonance frequencies) has emerged as one of the best instruments to characterize the thermodynamic behavior of a fluid through the speed of sound. This technique was developed by Moldover, Mehl and Greespan during the eighties [5], [6] and continued by Edwing and Trusler in the nineties [7], [8], among others; and whose acoustic model is described in section 2. For example, in our spherical resonator, described in section 3, quality factors $Q = \frac{f_N}{2g_N} = resonance\ frequency/\ line - width$ are obtained with values between 1956,3 (mode (0,6) at p=4MPa, T=300K) and 14294,2 (mode (0,4) at p=13MPa, T=300K), typically one order of magnitude above resonators of other geometries, e.g. those of cylindrical cavity. And above other techniques such as interferometers because at low frequencies these have large boundary effects that difficult the calculations with sufficient accuracy, while at high frequencies, these lose resolution since the resonance modes are not individually resolved (overlapping problems). The higher the Q, more sharp the resonance peaks will be, so best detection of the lines will be performed, resulting in greater accuracy of measurement. With this in our mind, the results obtained at three isotherms, 273K, 300K and 325K, and pressures range from 13MPa to 1MPa, are discussed in section 4 and compared with the GERG-2008 model.

2. Acoustical model.

The development of the acoustic-physical techniques for the thermodynamic characterization of fluids is found completely illustrated in [9]. In the study of the speed of sound in a fluid by a spherical resonator, the starting point is given by the equation:

$$c = \frac{2\pi a}{\nu_{ln}} f_{ln} \tag{1}$$

where a is the inner radius of the resonator cavity, ν_{ln} is the zero of the spherical Bessel first derivate of order l (these values are tabulated in [10]) and f_{ln} is the resonance frequency of propagation mode l,n of the acoustic wave. To achieve this result, it is solved the wave equation:

$$\frac{\partial^2 \Psi}{\partial t^2} = \frac{1}{c^2} \nabla^2 \Psi \tag{2}$$

$\Psi(\mathrm{r}, \mathrm{t})$ is the velocity potential. The fluid speed v can be separated in two components: a longitudinal one, v_l, irrotational $\nabla \times v_l = 0$, that can be expressed in term of the velocity potential as $v_l = -\nabla\Psi(\mathrm{r}, \mathrm{t})$ and a transversal one, v_r, that is rotational $\nabla \cdot v_r = 0$. v_l takes into account the propagation mode of the sound, while v_r is independent of ∇p_a and is ignored in the interior of the fluid, but it is important in the interphase region between the wall and the fluid to satisfy the boundary conditions. Here p_a indicates the perturbation to the thermodynamic equilibrium pressure p of the fluid by the presence of the acoustic wave (analogous for the acoustic contributions to the temperature T_a and the density ρ_a). Meanwhile, the fluid is assumed at rest and v is the acoustic magnitude itself. Looking for solutions of the harmonic waveform by simplicity, it is follow that:

$$\Psi(\mathrm{r}, \mathrm{t}) = \mathrm{A} \cdot \mathrm{f}(\mathrm{r}, \mathrm{t}) \tag{4}$$

where any wave function can be decomposed in an infinity series (or integral) of sines and cosines (of infinity frequency components: the fundamental one and all of its harmonics) by Fourier analysis. By the separation variables method $f_N(r,t) = \phi(r) \cdot \chi(t)$ and, as the temporal dependence is imposed by the acoustic source $\chi(t) = e^{j\omega_N t}$, being ω_N the angular frequency of the *N-th* component of the infinite set of natural frequencies (or normal modes) of the system. So the equation to be solved is (the Helmholtz equation):

$$(\nabla^2 + k^2)\phi_N(r) = 0 \tag{5}$$

where $k = \omega \cdot c$ is the propagation constant. If the spherical coordinates (r, θ, φ) are taken and $\phi_N(r)$ is separated like $\phi_N(r) = R_N(r)P_N(\theta)Q_N(\varphi)$, the following equation system is obtained:

$$\begin{gathered} \frac{1}{R}\frac{d^2R}{dr^2} + \frac{2}{rR}\frac{dR}{dr} + k^2 - \frac{l(l-1)}{r^2} = 0 \\ \frac{d^2P}{d\theta^2} + \frac{cos\theta}{sin\theta}\frac{dP}{d\theta} + \left[l(l-1) - \frac{m^2}{sin^2\theta}\right]P = 0 \\ \frac{d^2Q}{d\varphi^2} + m^2Q = 0 \end{gathered} \tag{6}$$

The solution of the angular components $P_N(\theta)Q_N(\varphi)$ are combined in the spherical harmonics:

$$P_N(\theta)Q_N(\varphi) = Y_{lm}(\theta, \varphi) \tag{7}$$

And the solution to the radial part is given by the spherical Bessel function of order *l*:

$$R_N(r) = j_l(k_N r) \tag{8}$$

The boundary condition imposed by the inner wall of the resonant cavity that must be accomplished by the wave function $\phi_N(r)$ confined in our geometry is:

$$v_n(r_s) = p_a(r_s)y(r_s, \omega) \tag{9}$$

being *n* the normal to the surface *S* of the resonator and $y(r_s, \omega) = \frac{y_0}{\rho c}$ the specific admittance on *S*. The relation between v_n and p_a is determined by the Navier-Stokes equation (linearized, on leading order approximation) for the longitudinal component of the fluid velocity as:

$$\frac{\partial v_l}{\partial t} = -\frac{1}{\rho}\nabla p_a + D_v\nabla(\nabla \cdot v_l) \tag{10}$$

When the frequency of the acoustic source (frequency of the forced acoustic oscillations) equals with the natural frequency of the cavity, a maximum in amplitude is obtained in the detector and a standing wave is formed, with a nodal surface on *S*, where $\nabla \cdot v_l$ is vanished. If equation (9) is inserted in (10) and it is expressed in terms of $\phi_N(r)$, it is concluded that:

$$\frac{\partial}{\partial n}\phi_N(r, \omega)|_{r=r_s} = -i\frac{\omega}{c}\phi_N(r_s, \omega)y(r_s, \omega) \tag{11}$$

where the admittance $y(r_s, \omega)$ takes into account all the effects of energy dissipation processes. In the ideal case $y(r_s, \omega) = 0$, so:

$$\frac{d}{dr}\phi_N(r)|_{r=a} = 0 \rightarrow \frac{d}{dr}j_l(k_N r)|_{r=a} = 0 \rightarrow k_n a = \nu_{ln} \tag{12}$$

that follows to the equation (1), with *n*=1,2,3.., *l*=0,1,2..n-1 and *m*=-*l*,…,+*l*. The measurements of speed of sound in a spherical resonator are taken studying preferably the radial symmetric modes, *l*=0, (the only no degenerated mode). In the real case, $y(r_s, \omega) \neq 0$, so a discrete set of complex values of the propagation constant (eigenvalues of the Helmholtz equation) are present in the form:

$$k_n = f_{0n} + ig_{0n} = \frac{c}{2\pi a}(\nu_{0n} + iy_s + ia\alpha) \tag{13}$$

where $Re\{k_n\}$ represents the resonance frequencies from which *c* is obtained and $Im\{k_n\}$ reports the half-widths of the resonances peaks. y_s is a complex magnitude, which imaginary component contributes to a shift Δf of the resonance frequency f_{0n}, then:

$$c = \frac{2\pi a}{\nu_{0n}}(f_{on} - \Delta f) \tag{14}$$

being f_{on} the experimental frequency. Strictly, such corrections depend on the corrected frequency itself, their behavior as corrector terms allows to approximate the dependence with the frequency to the experimental frequency f_{on}. The contributions implicated in y_s, following the steps detailed in [9] and [6], are:

2.1 Thermal Boundary Layer Admittance, y_{th}.

Consider the irreversible heat flows in the vicinity of the resonator walls due to the boundary conditions which imposes that the temperature and the heat flux are continuous in the interphase gas mixture - cavity (in fact, because the thermal conductivity and heat capacity of the shell are much greater than for the biogas, the conditions involve that the temperature is constant throughout the wall, without fluctuations). It causes a shift in the resonance frequency Δf_{th} and a contribution to the half-width g_{th}, as [11]:

$$\frac{\Delta f_{th}}{f} = \frac{-(\gamma-1)}{2a}\delta_{th}\frac{1}{1-l(l-1)/\nu_{ln}^2} + \frac{(\gamma-1)}{a}l_{th} + \frac{(\gamma-1)}{2a}\delta_{th,A321}\frac{\kappa_{Gas}}{\kappa_{A321}} \tag{15}$$

$$\frac{g_{th}}{f} = \frac{(\gamma-1)}{2a}\frac{1}{1-l(l-1)/\nu_{ln}^2}\delta_{th} + \frac{(\gamma-1)}{2a}\delta_{th,A321}\frac{\kappa_{Gas}}{\kappa_{A321}} \tag{16}$$

being:

l_{th}, the thermal accommodation length:

$$l_{th} = \frac{\lambda}{p}\left(\frac{\pi MT}{2R}\right)^{1/2}\frac{2-h}{h}\frac{1}{C_v/R+1/2} \tag{17}$$

where *h* is the thermal accommodation coefficient which is determined in [12].

δ_{th}, the thermal penetration length in the fluid, which characterized the thickness of the thermal boundary layer:

$$\delta_{th} = \left(\frac{\lambda}{\pi\rho C_{pf}}\right)^{1/2} \tag{18}$$

δ_{A321}, the thermal penetration length in the wall of the resonant cavity, which indicates the thickness of the thermal boundary layer in the shell (austenitic stainless steel A321):

$$\delta_{th,A321} = \left(\frac{\lambda_w}{\pi\rho_w C_{p,wf}}\right)^{1/2} \tag{19}$$

Our research, only interested in the radial symmetric modes *l=0*, thus the term $\frac{1}{1-n(n-1)/\nu_{ln}^2}$ is always equal to the unity. Since the wavelength λ is much greater than the thermal penetration length at the frequencies of our work, the temperatures gradients are larger in the thermal boundary layer than those in the fluid bulk, so the irreversible flows of heat are greater too. The frequency

shift f_{0n} were $-0{,}2\ Hz$ for the mode (0,2) and $-0{,}4\ Hz$ for the mode (0,6). Although it is generally expected to be the more important correction at low pressure measurements, it is the least of our corrections as seen below.

2.2 Coupling of Fluid and Shell Motion Admittance, y_{sh}.

It takes into account the mechanical admittance of the cavity wall by interaction between the acoustic waves with the corresponding shell motion. Even if this term can be exactly solved for an isotropic spherical resonator, as the elastic behavior model of the resonator developed in [13] and [6], it has been decided to use the simplified results show at [9], assuming that the radiation losses are null, because the system is allocated in high vacuum. Under this approximation, this correction term is pure complex, i.e., only contributes with a frequency shift Δf_{sh}:

$$\Delta f_{sh} = -f\rho c^2 C/[1-(f/f_{br})^2] \tag{20}$$

where:

C, the static compliance of the cavity:

$$C = \frac{1-\sigma}{2[(b/a)^3-1]\rho_{A321}c_{A321}^2}\left(\frac{(b/a)^3}{1-2\sigma}+\frac{2}{1+\sigma}\right) \tag{21}$$

f_{br}, the breathing frequency, it is the lower radial symmetric mechanical resonance of the shell:

$$f_{br} = \frac{c_{A321}}{2\pi a}\left(\frac{2[(b/a)^3-1]}{[(b/a)-1][1+2(b/a)^3]}\right)^{1/2} \tag{22}$$

being ρ_{A321} the density of the steel, σ the Poisson's ratio of the steel and c_{A321} the sound speed through the steel wall. The elastic properties of the steel A321 have been approximated by those of the steel of grade A304, because more reliable data are found in the literature of the latter. The two grades are very similar (although A321 is stabilized with Ti) and it is supposed that their mechanical behavior is equal, in our work ranges. The density, Young' moduli and Poisson's ratio data are taken from [14], the heat capacity and the thermal conductivity from [15] and the thermal expansion coefficient from [16]. The frequency shift of f_{0n} takes values from $-1{,}5\ Hz$ for the mode (0,2) and $-15\ Hz$ for the mode (0,6) at high pressures, to $-0{,}1\ Hz$ for the mode (0,2) and $-1\ Hz$ for the mode (0,6) at the lower pressures. Definitely it is the main correction term on f_{0n}, being that our biogas studied mixture is relatively dense (especially if it is compared with the references gases employed for the calibration of the resonator, such as Argon or Helium: the biogas is one order of magnitude heavier than Ar and two more than He).

2.3 Duct Admittance, y_0.

Corrector term due to the modification of the cavity surface admittance by the openings of the inlet biogas feed duct (y_0) is modeled by a cylindrical tube of radius $b = 0{,}5\ mm$ and length L= $41\ mm$, applying the Kirchhoff-Helmholtz theory for closed tubes finished in a rigid wall ($y_L = 0$), as is described in [9]:

$$\Delta f_0 + ig_0 = \frac{c}{2\pi a}\frac{\Delta S}{4\pi a^2} iy_o \tag{23}$$

where:

$$y_0 = itan(k_{KH}L) \tag{24}$$

$$k_{KH} = \frac{\omega}{c} + (1-i)\left(\frac{\omega}{2cb}[\delta_s + (\gamma-1)\delta_{th}]\right) \quad (25)$$

and being ΔS the area of the opening, $\delta_s = \left(\frac{2D_s}{\omega}\right)^{1/2}$ and $\delta_{th} = \left(\frac{2D_{th}}{\omega}\right)^{1/2}$, where $D_s = \eta/\rho$ and $D_{th} = \kappa/\rho C_p$ are the viscous (shear) and thermal diffusivities, respectively. See that it has been chosen a length tube (2 ducts in our experimental device: the inlet feed mentioned above and other blind tube with no function) similar to the radius resonator, with the objective of minimize the effect of this perturbation. The frequency shift is around $-0{,}4\ Hz$ for the mode $(0{,}2)$ and $-0{,}8\ Hz$ for the mode $(0{,}6)$ to this contribution, increasing slightly when both frequency and temperature are increased and pressure is reduced, in the ranges of our work.

2.4 Viscous Boundary Layer Admittance, y_s.

The admittance component because of the viscous boundary layer is zero for the radial symmetric modes (n=0), since the acoustic wave is normal incident on the wall and in absence of tangential motion, there is no viscous shear damping.

2.5 Dissipation in the Fluid.

The contribution to the half-width of the peak of resonance caused by the classical viscothermal mechanisms of acoustical energy absorption in the fluid bulk is given by:

$$g_{cl} = \left(\frac{c}{2\pi}\right)\left(\frac{\omega^2}{2c_0^3}\right)\left[\frac{4D_s}{3} + (\gamma-1)D_{th}\right] \quad (26)$$

As already stated, it has a minor effect than in the boundary layers, because temperature and velocity gradients are lower in the fluid bulk, with corresponding irreversible heat and momentum flows lower. Furthermore, this term is proportional to ω^2, versus the admittance component due to thermal boundary layer which increases only in proportion to $\omega^{1/2}$, being even less important at low frequencies.

2.6 Geometrical Imperfections.

In addition to the non-zero surface shell admittance y_s, there exist corrections over the ideality of the cavity by imperfect geometry, in the sense of perturbations of the perfect shell sphericity. As it is shown in [17], on leading order the effect of a smooth spherical distortion do not produce a frequency shift of f_{0n}, for the radial modes, if it is not change on the volume. It is unnecessary to apply a superior order correction, thus accuracy of *ppm* in the measurement of the speeds of sound, which is within the measurement uncertainty, can be reached with geometrical shape distortions of about 10 μm, feasible with the mechanical tolerances of conventional machining.

2.7 Virial Acoustic Equation.

Then, for the thermodynamic research of fluid properties, the speed of sound is related with the thermodynamic state by:

$$c^2 = \frac{\partial p}{\partial \rho}\Big|_S \quad (27)$$

expression valid only if it is not taken account any mechanism of dispersion, i.e., if $c(p,T)$ is frequently independent. Working at frequencies and densities sufficiently lower this is true, on first approximation: it is required that $\omega\tau_c \ll 1$, where for gas mixtures the mean time between binary collisions, τ_c, is close to the characteristic relaxation times of heat and momentum transfer,

$\tau_{th} = D_{th}/c_0^2$ and $\tau_s = D_s/c_0^2$, respectively. In our biogas sample $\tau_{th} \approx 2{,}5 \cdot 10^{-10} s$ and $\tau_s \approx 3 \cdot 10^{-10} s$ versus $\tau \approx 1{,}8 \cdot 10^{-4} - 4{,}8 \cdot 10^{-5}\ s$, so the requirement is properly met. The equation (27) can be expressed in terms of variables (p, T) and (ρ, T):

$$c^2 = \left[\left(\frac{\partial \rho}{\partial p}\right)_T - \frac{T}{\rho^2 C_p}\left(\frac{\partial \rho}{\partial T}\right)^2_p\right]^{-1} \tag{28}$$

$$c^2 = \left[\left(\frac{\partial p}{\partial \rho}\right)_T - \frac{T}{\rho^2 C_v}\left(\frac{\partial p}{\partial T}\right)^2_\rho\right] \tag{29}$$

The measurements are fitted to the acoustic virial equation of state, explicit in pressure or in density:

$$c^2 = A_0 + A_1 p + A_2 p^2 + \cdots \tag{30}$$

$$c^2 = A_0(1 + \beta_a \rho + \gamma_a \rho^2 + \cdots) \tag{31}$$

where the first acoustic parameter provide important information in the limit of perfect gas, $p \to 0$:

$$A_0 = \frac{RT\gamma^{pg}}{M} \quad \rightarrow \quad \frac{C_{p,m}^{pg}}{R} = \frac{\gamma^{pg}}{\gamma^{pg}-1} \tag{32}$$

where the superscript "*pg*" indicates perfect gas, R is the gas constant, M is the mean molar mass, T is the thermodynamic temperature and γ is the adiabatic coefficient. As it is shown in [6], when proceeding to acoustic virial equation regression is necessary to choose those resonance modes which frequency far enough of mechanical resonances, the breathing modes of the shell, since it is avoided a high energy transfer from the acoustic wave through the cavity wall. If not the acoustical model developed is not valid. So the frequency limit for our resonator is $f_{br} \approx 27500\ Hz$, such that the research is constraint to the first five radial modes of the speed of sound in the biogas.

3. Experimental equipment and process of measurement.

3.1 Resonant Cavity.

The spherical resonator used in this work is directly based on the designs developed by Trusler and Ewing [18] and employed recently in other research [19]. Built with the objective to perform the highest possible absolute accuracy speed of sound measurements, it consists of a spherical cavity formed by the union of two aligned hemispheres and fixed by electron beam welding, fabricated from austenitic stainless steel of grade 321 and manufactured at Imperial College, with nominal radius $a = 40mm$ and nominal thickness $b - a = 10mm$.

The determination of the cavity geometry, the average inner radius as function of the pressure and temperature required for the calculation of the speed of sounds, was made in a previous work [19] by means of calibration with argon, because there is well-known equation of state for this gas. Some authors have reported several problems with the junction of the hemispheres [20]: the welding do not fill all the thickness of the shell, just about $6mm$ of the wall and the cavity has not been subjected to annealing or other later thermal treatment, which suggests to the authors that the union is causing a small additional geometric imperfection and irreversible changes in the mean radius

after following a temperature cycle. On the other hand, the machining and polishing of the steel block from the two hemispheres are obtained, produce a maximum imperfection on the geometry that affects in 2 parts in 10^4 the inner radius a [21] and, due to the reasons given previously, it is neglected.

Typically, it is used stainless steel instead of aluminum or brass, because has a higher value of the characteristic acoustic admittance $\rho_w c_w$ and reduce the correction term for coupling the fluid and shell motion, and the austenitic type because being nonmagnetic, needful to determine the radius by microwave resonance study.

The employed shell comprises two openings: one for the inlet/outlet duct, drilled and sealed with an stainless steel O-ring in the upper boss, of radius $0{,}5mm$ and length $41mm$, and the other one is a blind tube in the lower boss, of the same dimensions that the former one.

3.2 Transducers.

Flush with the inner surface of the north shell hemisphere, it is disposed two equals transducers of wide bandwidth, source and detector, provided in an angle of 90° between them (this angle reduces the overlapping between the radial mode (0,2) and the very close degenerated mode (3,1), since the detector is located in a nodal plane respect to the latter mode) and they follow the design showed in [22].

They are capacitance transducers which consist of a solid polymeric dielectric (a polyamide circular sheet) of $12\mu m$ thickness and $3mm$ diameter, coated with a gold layer of $50nm$ thickness on the side facing the interior of the shell. The whole creates a moving part, the diaphragm, that it is placed on a massive back electrode, joined by a spring to the transducer cover to keep it aligned inside the ceramic tube that adjust all the dispositive to the shell. The diaphragm is provided with a little perforation to allow the pass of the gas to the interior volume of the transducer, thereby decreases the rigidity and increases the sensitivity of the transducer, which is given by: $\frac{V}{p_a} = E_0 \frac{\langle \xi \rangle}{p_a}$, being $\langle \xi \rangle$ the mean amplitude of the diaphragm displacement. They are designed so that the mechanical resonance frequencies of the diaphragm are well above the acoustic ones of the cavity, so there are no overlapping problems, typically, they have a minimum mechanical resonance value around $40\ kHz$.

The source transducer is driven by a pure alternate signal send out by the wave generator HP3225B, without bias voltage, $V_0 = 0$, to avoid the direct electromagnetic coupling between the two transducers, "crosstalk" effect, and producing an acoustic pressure response at twice the frequency of the wave synthesizer. The net force on the diaphragm is given by: $F = -\left(\frac{\varepsilon_0 \mathrm{A}}{2}\right)\left(\frac{V_0 + V_1 \cos(\omega t)}{d_0 + d_1/\varepsilon_r}\right)^2 \rightarrow F = -\left(\frac{\varepsilon_0 \mathrm{A}}{2}\right)\left(\frac{{V_1}^2 + {V_1}^2 \cos(2\omega t)}{2(d_0 + d_1/\varepsilon_r)^2}\right)$, where A is the diaphragm area, ε_r is the dielectric permittivity of the polymer, d_1 is the thickness of the diaphragm and d_0 is the separation between the back electrode and the diaphragm at $\omega = 0$. It operates with rms voltage of $180V$ on the source, delivered by rise signal amplifier because the wave generator only contributes with $40V$, with a precision in the frequencies of $1 \cdot 10^{-7} f$, as indicated by the manufactured, but the synthesizer is plugged to a rubidium standard frequency, that improves the precision until $5 \cdot 10^{-11} f$.

The transducer detector is fed with a bias voltage of $85V$ whose exit signal is supplied to an amplifier detector Lock-In SR850 DSP, after passing through a unity gain amplifier and high input impedance with the purpose of delete the effect of the capacitance connection cables (triaxial cable with active guard): the transducer capacitance C_T is small enough (less than $100pF$) such that a

little load capacitance C_L, like the connection cables, involves a high division of the output signal by $(C_L + C_T)/C_L$. The Lock-In is referenced to the second harmonic of the driven source signal and measures the amplitude and shift phase of the detector signal, with amplitudes between $10\mu V - 200\mu V$, performed by acoustic pressure levels of $1mPa - 20mPa$, together with noise electronic levels of $50nV$ rms.

3.3 Measurement of Pressure and Temperature.

The pressure measurement is performed with a piezoelectric quartz transducer, Digiquartz 43RK-101, placed on the top of the biogas inlet tube, so the hydrostatic column correction is taken account by measuring the temperature of three thermocouples located each $20cm$ of the filling gas duct (which has a $61cm$ length between the equatorial plane of the resonant cavity and the top pressure transducer). It is calibrated from $1MPa$ to $20MPa$ in TermoCal labs, with national traceability. The overall estimated uncertainty in pressure is $\pm 2 \cdot 10^{-3} MPa$ with a cover factor of *k=2*.

The temperature measurement of the resonator is performed with two standard platinum resistance thermometer, SPRT Rousemont 162D of 25.5Ω with Inconel X-750 encapsulated in four wire configuration, placed on the north and south hemispheres (in copper blocks and covered by thermal grass) plugged to an ac bridge ASL F18, referenced to external resistance Tinsley 5685ª (of 25Ω nominal, thermostated at $36°C$ and calibrated at INTA, Instituto Nacional de Técnica Aeroespacial).The two SPRT are calibrated in ITS-90 scale at TermoCal labs with national traceability. These measurements are not employed in the temperature control system because the long stabilization time of the ac bridge. The overall estimated uncertainty in temperature is $\pm 2 \cdot 10^{-3} K$ with a cover factor of *k=2*.

3.4 Control System of the Thermal Stability.

It is very important to control the thermal stability of the resonator before making each measurement. On one hand, the resonant cavity is suspended within an interior cylindrical stainless steel jacket, which is only linked by a copper block, as shown in Figure 1. Said jacket is communicated with the outer cylindrical vessel, stainless steel also, and this one is connected through the tube connections with the centrifugal vacuum pump Leybold Trivac B8B, helped by a turbomolecular pump Leybold SL300 in series with previous one, to reach pressures about $10^{-3} Pa$ and deleting convection in the two chambers. The exterior vessel is bolted to the cover of the top support tube and maintains the high vacuum through a joint of indium. On the other hand, between the jacket and the vessel, several aluminum layers over fiberglass with all possible wiring inside surrounds the jacket minimizing the radiation losses. The entire assembly is allocated in a Dewar, filled with ethanol and cooled by a thermal bath Julabo FP89 at $-30°C$, trying to transmit heat exclusively by thermal conduction through the copper block on the top.

The temperature is stablished using three resistors: a band resistance of 10.6Ω in the copper block in order to heat the resonant shell, a wire resistance of 28.5Ω wound along the side of the jacket and three band resistances forming a triangle of 174Ω at the base of the jacket, in order to compensate the radiation losses indicated previously. And the temperature is controlled with three other probes: a SPRT Rosemount 162D Pt-25 attached by a cooper envelope to the copper block and two SPRT Hart 5686 Pt-25 stuck with thermal tape to the side and base of the jacket. The entire system is automated by three independent control loops implemented with PC Agilent VEE 7.0, which monitors the temperatures measured taken in the multimeter HP 3458A and the programmable power supplies HP E3632A plugged to the corresponding resistances.

Usually, the whole apparatus takes to stabilize a day after each pressure drop, carried out in ramps of about 10 MPa, and about five days after each new assignment of reference temperature, ran at around $25\,K$ ramps. With this thermostated device, a thermal gradient between the two cavity hemispheres only of $1mK$, with even lower drifts, is achieved during the measurement process.

3.5 Resonance Measurement System.

It was implemented in two independent programs, under PC Agilent VEE 7.0 and adapted in the laboratory, taken as base the software developed at Imperial College for similar experimental device. It consists of a first program which goal is to sweep over wide frequency ranges and locate all the resonances peaks in that range, indicating the frequency f_N and the half-width g_N of the most significant. Thus, it can be quickly estimate the series of radial resonance modes if looking around the theoretically predicted frequencies. The second program performs the measurement of radial resonance mode with the highest accuracy, requiring from the frequency of the peak provided by the previous software. This measurement is done by tracking the amplitude A and phase φ detected by the Lock-In amplifier, i.e, the signal in phase $u = A\cos\varphi$ and the signal in antiphase $v = A\sin\varphi$, at 11 points equally spaced in the interval $[f_N - g_N, f_N + g_N]$, in a ramp up and down, waiting a few seconds between each point to ensure the stationary of the received signal at the Lock-In. A total of 11 frequencies and 44 voltages that fit a function of the form $u + iv = \sum_N \frac{if A_N}{(f^2 - F_N^2)} + B + C(f - f_0)$ with $A_N, B\ and\ C$ complex constants and with $N = 1$ for the radial symmetric modes, obtaining the complex frequency values $F_N = f_N + ig_N$, with lower frequency deviations of $0.01 \cdot f_N$ %.

3.6 Biogas Mixture.

The biogas mixture sample was prepared at Reference Materials Laboratory of CEM (Centro Español de Metrología) by the gravimetric method to the technical procedure CEM-PT-0121, according to standard UNE-EN ISO 6142, with the compositions shown in Table 1. After the preparation, the mixture composition was verified, by comparison with MRP, following the technical procedure CEM-PT-0122.

Table 1 Mixture compositions of biogas sample.

Composition	Concentration / 10^{-2} mol/mol	Uncertainty / 10^{-2} mol/mol (k=2)
CO	4,9899	0,0050
CO_2	35,1484	0,0023
N_2	10,0138	0,0040
CH_4	49,8478	0,0069

3.7 Ranges of Operation.

The resonator thermostated system it was designed to operate within the range from 123K to 523K, though our research is limited at three isotherms: 273K, 300K y 325K. The resonator is built to work until 20 MPa, but our measurements are focused from a maximum pressure of 12 MPa decreasing by steps of 1 MPa to a minimum around 1 MPa. Generally, the upper limit is imposed by the pressure in the sample biogas bottle, incremented by a manual piston cylinder system in some MPa, after several consecutive loads.

4. Results.

The experimental results of the speed of sound are shown in Tables 2-4 together with the corresponding theoretical values determined using the equation of state (EoS) GERG-2008, now standard for biogas mixtures [23] - [24]. EoS GERG-2008, with the default settings of the reference fluid properties software NIST Refprop 9.1 [25], was used. The default values of the equation of state are not those of the originally model GERG published at [23] for the pure fluids, but a more complex and long version, slightly more accurate, as it is indicated by the help of the software.

Not all radial symmetric modes have been used to calculate the average value of $c(p,T)$ in each state, but the relative excess half-widths of the resonance peaks $\Delta g/f_{exp} = (g - (g_{th} + g_{cl} + g_0))/f_{exp}$, which should match with the contribution of vibrational relaxation g_{rel}, are plotted versus the pressure in Figure -3. Thus, the Figure shows that the mode (0,5) must be discarded from the calculations at $T_{nominal}$=273 K, because $\Delta g/f_{exp}$ is very high in the entire range of pressures and also the mode (0,6) should be removed from calculations, because $\Delta g/f_{exp}$ does not tend to vanish with decreasing pressure. For the same reasons, modes (0,5) and (0,6) are also excluded at $T_{nominal}$=300 K and mode (0,6) at $T_{nominal}$=325 K, as shown in Figure 2 and 3.

Table 2 Experimental speeds of sound with their corresponding expanded uncertainties (k=2) at $T_{nominal}$=273K and comparison with EoS GERG-2008.

P / MPa	T / K	c_{exp} / m·s^{-1}	c_{GERG} / m·s^{-1}	$(c_{exp} - c_{GERG})/c_{exp}$ / ppm
11.586	272.969	313.325±0.054	314.423	3504.476
10.161	272.971	305.003±0.014	305.705	2304.727
9.127	272.966	301.896±0.017	302.440	1802.811
8.187	272.967	300.953±0.013	301.403	1496.566
7.155	272.960	301.593±0.042	301.962	1225.496
6.118	272.959	303.617±0.021	303.914	979.922
5.065	272.954	306.716±0.020	306.943	738.250
4.055	272.962	310.407±0.021	310.567	514.551
3.039	272.954	314.609±0.017	314.709	317.936
2.015	272.957	319.208±0.034	319.257	151.724
1.021	272.961	323.890±0.091	323.928	116.959

Table 3 Experimental speeds of sound with their corresponding expanded uncertainties (k=2) at $T_{nominal}$=300K and comparison with EoS GERG-2008.

P / MPa	T /K	c_{exp} / m·s^{-1}	c_{GERG} / m·s^{-1}	$(c_{exp} - c_{GERG})/c_{exp}$ / ppm
12.826	299.852	339.58±0.12	339.67	283.22
12.074	299.846	335.910±0.086	335.979	205.577
11.030	299.845	331.96±0.19	331.96	-19.86
10.161	299.849	329.569±0.070	329.558	-32.783
9.104	299.842	327.727±0.035	327.716	-32.987
8.079	299.848	326.977±0.024	326.965	-36.887
7.061	299.838	327.107±0.049	327.086	-63.261
6.062	299.850	327.995±0.020	327.957	-114.187
5.050	299.841	329.512±0.015	329.449	-190.200
4.029	299.850	331.604±0.021	331.508	-287.234
3.020	299.850	334.108±0.066	333.977	-392.215
2.010	299.851	336.969±0.061	336.814	-459.100
1.004	299.845	340.098±0.095	339.948	-441.680

Table 4 Experimental speeds of sound with their corresponding expanded uncertainties (k=2) at $T_{nominal}$=325K and comparison with EoS GERG-2008.

P / MPa	T /K	c_{exp} / m·s^{-1}	c_{GERG} / m·s^{-1}	$(c_{exp} - c_{GERG})/c_{exp}$ / ppm
11.094	324.749	351.127±0.096	351.064	-181.904
10.035	324.740	348.922±0.063	348.798	-353.741
9.082	324.743	347.514±0.037	347.395	-342.726
8.094	324.741	346.645±0.024	346.524	-350.873
7.055	324.744	346.331±0.054	346.202	-372.327
6.056	324.744	346.560±0.067	346.413	-423.518
5.043	324.744	347.263±0.072	347.095	-485.167
4.045	324.744	348.38±0.12	348.18	-568.87
3.031	324.743	349.877±0.089	349.655	-636.170
2.038	324.748	351.675±0.073	351.431	-695.807
1.011	324.742	353.82±0.12	353.57	-716.91

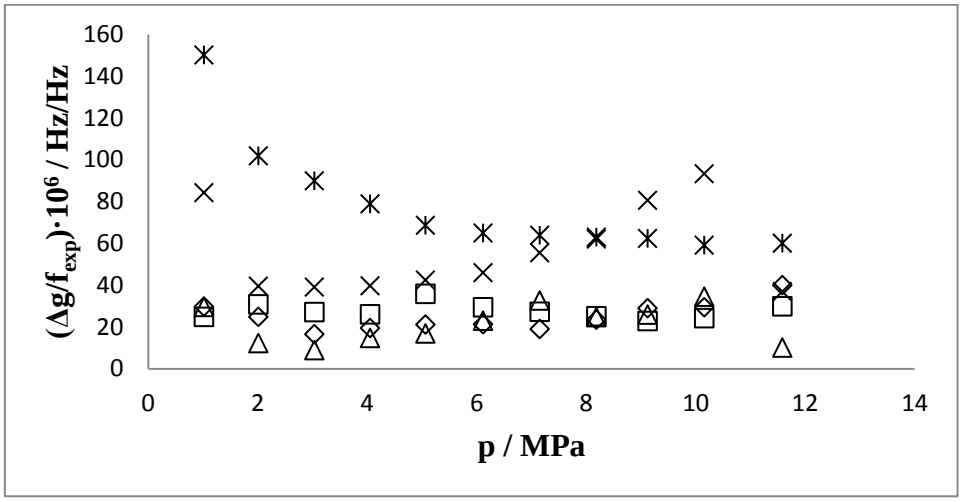

Figure 1 Relative excess half-width ($\Delta g/f_{exp}$) of radial modes as function of pressure at $T_{nominal}$=273 K for modes: ◇ (0,2), □ (0,3), △ (0,4), × (0,5), ∗ (0,6).

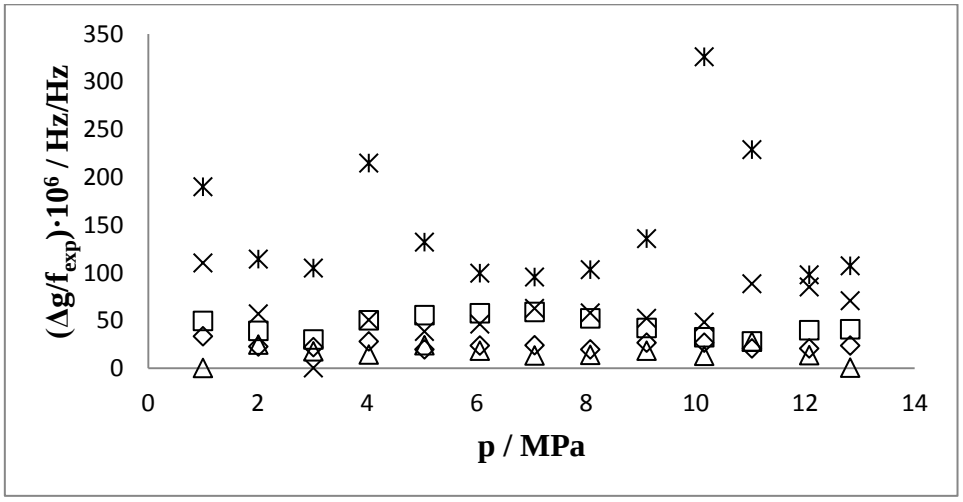

Figure 2 Relative excess half-width ($\Delta g/f_{exp}$) of radial modes as function of pressure at $T_{nominal}$=300 K for modes: ◇ (0,2), □ (0,3), △ (0,4), × (0,5), ∗ (0,6).

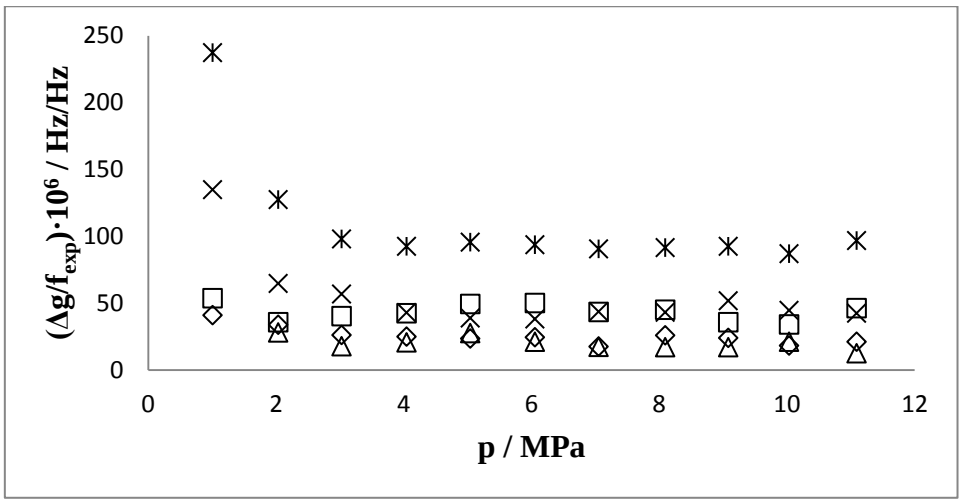

Figure 3 Relative excess half-width ($\Delta g/f_{exp}$) of radial modes as function of pressure at $T_{nominal}$=325 K for modes: ◇ (0,2), □ (0,3), △ (0,4), × (0,5), ∗ (0,6).

In Table 5 the fitting parameters of the square speed of sound to the acoustic virial equation (equation 30) are shown. The residual of the fitted speed of sound in comparison to the calculated values using EoS GERG-2008 were determined in order to choose the truncation orders of the pressure expansion. Comparing the standard deviation $\sigma = \sqrt{\sum(x - \bar{x})^2 / (n-1)}$ of the n residuals $x = (c_{\text{fitted}} - c_{\text{GERG}})/c_{\text{fitted}}$, it is concluded that third order acoustic model for isotherms $T_{nominal}$=273K and $T_{nominal}$=300K and second order for the isotherm $T_{nominal}$=325K are necessary; the inclusion of a new term is negligible as it is shown in Table 6 for the different fittings to acoustic virial equations. The Table 5 also contains the parameters expanded uncertainties for a cover factor k=2 calculated through Monte Carlo method, as indicated in [26].

Table 5 Fitting parameters of square speed of sound and their corresponding expanded uncertainties (k=2).

$T_{nominal}$ / K	$A_0(T)$ / $(m/s)^2$	$A_1(T)$ / $(m/s)^2\cdot Pa^{-1}$	$A_2(T)$ / $(m/s)^2\cdot Pa^{-2}$	$A_3(T)$ / $(m/s)^2\cdot Pa^{-3}$
273	107499±85	$(-250{,}1\pm4{,}5)\cdot10^{-5}$	$(-170{,}2\pm7{,}1)\cdot10^{-12}$	$(272{,}7\pm3{,}5)\cdot10^{-19}$
300	117816±94	$(-219{,}0\pm5{,}4)\cdot10^{-5}$	$(16{,}43\pm9{,}0)\cdot10^{-12}$	$(108{,}4\pm4{,}4)\cdot10^{-19}$
325	127439±77	$(-219{,}7\pm2{,}7)\cdot10^{-5}$	$(162{,}8\pm2{,}1)\cdot10^{-12}$	-

Table 6 Standard deviations (σ) of the residuals of the different fittings to the acoustic virial equation.

	σ $[(c_{fitted} - c_{GERG})/c_{fitted}]$ / ppm			
$T_{nominal}$ / K	$c^2(p,T) = A_2(T)\cdot p^2 + A_1(T)\cdot p + A_0(T)$	$c^2(p,T) = A_3(T)\cdot p^3 + A_2(T)\cdot p^2 + A_1(T)\cdot p + A_0(T)$	$c^2(p,T) = A_2(T)\cdot p^2 + A_1(T)\cdot p + A_0(T) + b(T)\cdot p^{-1}$	$c^2(p,T) = A_4(T)\cdot p^4 + A_3(T)\cdot p^3 + A_2(T)\cdot p^2 + A_1(T)\cdot p + A_0(T)$
273	4469,0	1163,9	2918,7	1038,7
300	1964,9	250,6	1207,7	230,6
325	580,5	168,5	356,7	168,9

The thermodynamics properties derived from measurements of speed of sound in the limit to zero pressure, as prefect gas “pg”, are shown in Table 7 to 9 for biogas sample mixture: the adiabatic

coefficient γ^{pg}, the isochoric and isobaric heat capacities C_V^{pg} and C_p^{pg} and the acoustic virial coefficients β_a and γ_a. The results are compared with those reported by the software REFPROP 9.1 (updated to the last version at June 10, 2014) using EoS GERG-2008 (standard for our fluid), AGA-8 and Peng-Robinson (PR). If we focus at the properties determined from $A_0(T)$, i.e., γ^{pg}, C_V^{pg} and C_p^{pg}, the correlation to a cubic acoustic virial equation is more satisfactory for $T_{nominal} = 300K$ than the cubic fitting for $T_{nominal} = 273K$ or square fitting for $T_{nominal} = 325K$, because we move from a relative deviation about 1% to a relative difference with the theoretical values of 0,1%, being within the measurement uncertainty in the latter case. For the second acoustic virial coefficient, relative deviations between the theoretical results calculated by any of the three equations of state no matter the isotherm and those measured are very similar and around 20%, i.e., two orders of magnitude above the measurement uncertainty but in agreement with other works [19]. However, the third acoustic virial coefficient calculation, performed by software REFPROP 9.1, fails to determine its value using EoS GERG-2008, which seems to be an error of the calculation algorithm and not a problem with the model. The theoretical estimation given by EoS AGA-8 or Peng-Robinson (PR) is several times the experimental data above itself when it is utilized the cubic correlation ($T_{nominal} = 273K$ and $T_{nominal} = 300K$), but relatively close for the square fitting ($T_{nominal} = 325K$).

Table 7 Thermodynamic derived properties from first acoustic virial coefficient (equation 31 and 32) at $T_{nominal}$=273K with their corresponding expanded uncertainties (k=2) and comparison with the different EoS.

$T_{nominal}$=273K	Z_{exp}	$(Z_{exp}- Z_{GERG})/Z_{exp}$ %	$(Z_{exp}-Z_{AGA})/Z_{exp}$ %	$(Z_{exp}- Z_{PR})/Z_{exp}$ %
γ^{pg}	1.3105±0.0011	-0.64	-	-
C_v^{pg} / Jmol^{-1}K^{-1}	26.774±0.091	2.62	-	-
C_p^{pg} / Jmol^{-1}K^{-1}	35.09±0.12	2.00	-	-
β_a / m^{3}mol^{-1}	(-528.0±9.5)·10^{-7}	-29.67	-35.62	-39.56
γ_a / (m^{3}mol^{-1})^2	(-81.5±3.4)·10^{-10}	$1.72 \cdot 10^9$	192.28	325.43

Table 8 Thermodynamic derived properties from first acoustic virial coefficient (equation 31 and 32) at $T_{nominal}$=300K with their corresponding expanded uncertainties (k=2) and comparison with the different EoS.

$T_{nominal}$=300K	Z_{exp}	$(Z_{exp}- Z_{GERG})/Z_{exp}$ %	$(Z_{exp}- Z_{AGA})/Z_{exp}$ %	$(Z_{exp}- Z_{PR})/Z_{exp}$ %
γ^{pg}	1.3075±0.0011	-0.06	-	-
C_v^{pg} / Jmol^{-1}K^{-1}	27.036±0.094	0.25	-	-
C_p^{pg} / Jmol^{-1}K^{-1}	35.35±0.13	0.19	-	-
β_a / m^{3}mol^{-1}	(-46.3±1.1)·10^{-6}	-9.61	-15.10	-17.91
γ_a / (m^{3}mol^{-1})^2	(8.7±4.8)·10^{-10}	$-1.11 \cdot 10^{10}$	-688.40	-1769.54

Table 9 Thermodynamic derived properties from first acoustic virial coefficient (equation 31 and 32) at $T_{nominal}$=325K with their corresponding expanded uncertainties (k=2) and comparison with the different EoS.

$T_{nominal}$=325K	Z_{exp}	$(Z_{exp}- Z_{GERG})/Z_{exp}$ %	$(Z_{exp}- Z_{AGA})/Z_{exp}$ %	$(Z_{exp}- Z_{PR})/Z_{exp}$ %
γ^{pg}	1.30590±0.00082	0.58	-	-
C_v^{pg} / Jmol^{-1}K^{-1}	27.180±0.073	-2.53	-	-
C_p^{pg} / Jmol^{-1}K^{-1}	35.495±0.098	-1.94	-	-
β_a / m^{3}mol^{-1}	(-465.5±5.7)·10^{-7}	19.03	14.69	13.30
γ_a / (m^{3}mol^{-1})^2	(93.1±1.2)·10^{-10}	$-7.48 \cdot 10^8$	31.46	-56.24

In Figure , the relative deviations of measures $c(p,T)$ with respect to the theoretical calculations by EoS GERG-2008 are shown. The biggest differences are obtained at high pressure ($P = 12MPa$) and low temperature ($T = 273K$), where the results of model GERG-2008 overestimate in an order of magnitude of $10^3 ppm$ the research data; then they are slightly reduced until to become cancelled at intermediate pressure and temperature ($P = 6\,MPa\;and\;T = 300K$) being within the measurement uncertainty; and they are increased again at high temperature ($T = 325K$) and low pressure ($P = 1\,MPa$), where in this case the model GERG-2008 underestimates about $10^2 ppm$ our measurements.

Firstly, the orders of magnitude of the deviations from the EoS GERG-2008 are within expected: when the relative differences of this study are compared with those obtained in similar mixtures (binary mixtures of CH4+N2 at related compositions) from reliable works [3], the average relative deviations are around $10^2 ppm$, in a wide range of pressures and temperatures (with the exceptions and trends that will be described below). Exactly, the research in [3] obtained an average deviation $\Delta_{average} = 600ppm$ at the sample {(1-x)·CH_4+x·N_2} with $x = 0{,}5422$, parallel to that stablished for the mixture CH_4+N_2+CO+CO_2 (Table 1) reported in these lines: $\Delta_{average} = 200ppm$.

In addition, this behavior of the speed of sound is analogous to that described in [27] for the density in a similar mixture (synthetic coal methane mine mixtures, CMM): it is reported that the density computed by EoS GERG-2008 also overestimate the experimental data, performed with a single Juncker densimeter with magnetic suspension. The relative deviation takes a maximum at the inferior temperatures ($\sim 250K$) and the superior pressures ($\sim 12MPa$), decreases passing through zero at the middle pressure and temperature range and increases again, underestimating the measurements at higher temperature ($\sim 375K$) and lower pressure ($\sim 1MPa$), just like in our work. However, in [27] measurements at various pressures above those of our experiment were performed, showing how the behavior was reversed: the relative differences between EoS GERG-2008 and experimental data took a new trend decreasing for the lowest isotherms ($250K$) and increasing for the highest temperatures ($375K$) for the pressure range from $12MPa$ up to $20MPa$. We suppose that speed of sound at higher pressures than those of this research follows the same trend as shown in [27] for the density, since both thermodynamic properties, related by equations (28 or 29), were taken as fundamental source of experimental data to model correlations of EoS GERG-2008 [24].

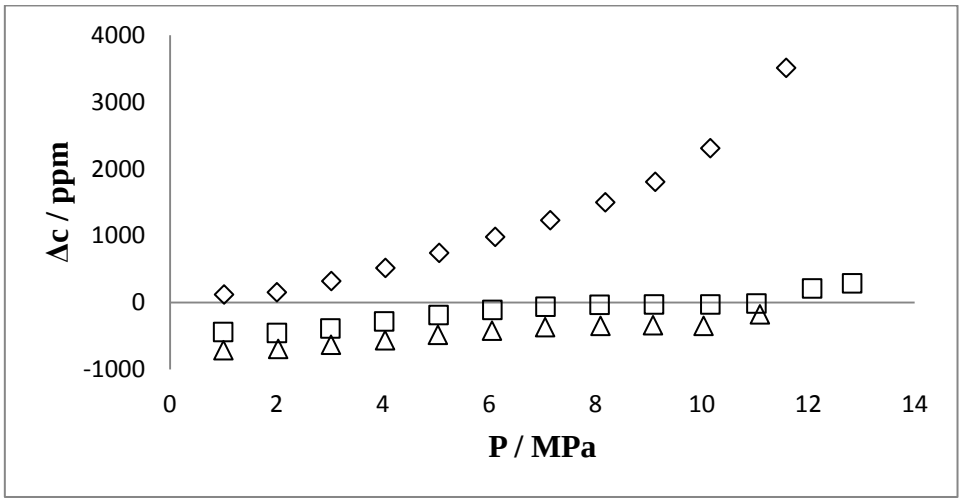

Figure 4 Relative deviations $\Delta c = (c_{GERG\text{-}2008}\text{-}c_{exp})/c_{exp}$ as function of pressure at $T_{nominal}$=273 K (◇), $T_{nominal}$=300 K (□), $T_{nominal}$=325 K (△).

5. Conclusions.

The speed of sound through a quaternary synthetized biogas-like mixture of CH_4+N_2+CO_2+CO has been measured with uncertainties better than $0.12\ m \cdot s^{-1}$ ($< 350 \cdot 10^{-6} \cdot c$), within the order of magnitude of other works: [2], [3] or [19]. These experimental data have been fitted to the acoustic virial equation, with three parameters, A_0, A_1 and A_2 at the isotherm $T_{nominal}$=325K and with four parameters, A_0, A_1, A_2 and A_4, at the isotherms $T_{nominal}$=273K and $T_{nominal}$=300K, obtaining relative uncertainties between $0.1\ and\ 6$ %.

Then some important thermodynamic properties have been derived and compared with the calculations from the current reference equation of state for our mixture, GERG-2008 using RefProp 9.1: the adiabatic coefficient γ^{pg} which deviates less than 0.6 %, the isochoric heat capacity as perfect gas C_v^{pg} which differs less than 2.5 % and the isobaric heat capacity as perfect gas C_p^{pg} which disagree less than 2 %. Second and third acoustic virial coefficients are discussed according the calculations using EoS AGA-8 and EoS Peng-Robinson, in addition to EoS GERG-2008, obtaining disparate results that do not adequately represent the experimental data in any condition.

The speed of sound behavior is closer to that modeled by EoS GERG-2008 at intermediate temperature and pressure ($P = \sim 6\ MPa\ and\ T = 300K$), but smoothly tends to disagree either at low temperature and high pressure ($P = 12MPa$ and $T = 273K$) or at the reverse state, high temperature and low pressure ($P = 1\ MPa$ and $T = 325K$), with deviations up to $10^3 ppm$. This is the same trend as described in the work [27] for the density of a similar mixture and it is expected that this difference begins to decrease with increasing pressure above our upper limit at 12MPa, like in [27]. Although, the measurements are within the limits of uncertainty claimed by the EoS GERG-2008, which is up to 0.1 % [24], this research is intended to describe how well the model works, as well as provide accurate experimental data to improve it.

References.

[1] Bob Flach, Karin Bendz and Sabine Lieberz, «EU Biofuels Annual 2014,» USDA Foreign Agricultural Service, 2014.

[2] J. P. M. Trusler, «The speed of sound in ($0{,}8CH_4$+$0{,}2C_2H_6$) at temperatures between 200K and 375K and amount of substance densities up to 5 mol·dm^{-3}.,» *Journal of Chemical Thermodynamics,* vol. 26, pp. 751-763, 1994.

[3] J. F. Estela-Uribe. et al, «Speeds of sound in {(1-x)CH_4 + xN_2} at temperatures between 170K and 400K and pressures up to 30 MPa,» *Journal of Chemical Thermodynamics,* vol. 38, pp. 929-937, 2006.

[4] R. M. Gavioso et al, «Measuring Humidity in Methane and Natural Gas with a Microwave Technique,» *International Journal of Thermophysics,* 2014.

[5] J. B. Mehl and M. R. Moldover, «Precision acoustic measurements with a spherical resonator: Ar and C2H4,» *Journal of Chemical Physics,* vol. 74, 1981.

[6] M. R. Moldover, «Gas-filled spherical resonators, theory and experiment,» *Journal of Acoustical Society of America,* vol. 2, nº 79, pp. 253-272, 1986.

[7] M. B. Edwing et al, «Speeds of Sound in CF_4 between 175 and 300K measured with a spherical resonator,» *Journal of Chemical Physics,* vol. 90, nº 2, pp. 1106-1115, 1989.

[8] M. B. Edwing et al, «Speeds of sound, perfect-gas heat capacities, and acoustic virial coefficients for methane determined using a spherical resonator at temperatures between 255K and 300K and pressures in the range 171kPa to 7.1MPa,» *Journal of Chemical Thermodynamics,* vol. 24, pp. 1257-1274, 1992.

[9] J. P. M. Trusler, Physical Acoustics and Metrology of Fluids, Adam Hilger, 1991.

[10] J. Olver F. W, Royal Society Mathematical Tables Volume 7: Bessel Functions part III, Cambridge University Press, 1960.

[11] G. Sutton, «Determination of the Boltzman constant: Acoustic models and corrections for Argon and Helium,» *NPL Report ,* nº 19, 2009.

[12] ..., «h».

[13] J. B. Mehl, *Journal of Acoustical Society,* vol. 78, p. 782, 1985.

[14] H. M. Ledbetter et al, «Low-temperature elastic properties of four austenitic stainless steel,» *Journal of Applied Physics,* vol. 46, pp. 3855-3860, 1975.

[15] «Solid Materials Database,» [En línea]. Available: https://botturl.web.cern.ch/botturl/CryoSoft/solids.html. [Last acces: 06 2015].

[16] «Cryogenic Technologies Group,» [En línea]. Available: http://cryogenics.nist.gov/MPropsMAY/304Stainless/304Stainless_rev.htm#le. [Last acces: 06 2015].

[17] J. B. Mehl, «Acoustic resonance frequencies of deformed spherical resonators,» *Journal of Acoustical Society of America,* vol. 79, nº 2, pp. 278-285, 1986.

[18] M. B. Edwing et al, «Speeds of Sound in CF4 between 175 and 300 K measured with a spherical resonator,» *Journal of Chemical Physics,* vol. 90, nº 2, pp. 1106-1115, 1989.

[19] F. J. Pérez- Sanz, «Speeds of Sound in ($0.95N_2$+0.05CO and $0.9N_2$+0.1CO) gas mixtures at T=(273 and 325) K and pressure up to 10 MPa,» *Journal of Chemical Thermodynamics,* vol. 79, pp. 224-229, 2014.

[20] A. F. Estrada-Alexanders et al, «The speed of sound in gaseous argon at temperatures between 110 K and 450 K and at pressures up to 19 MPA,» *Journal of Chemical Thermodynamics,* vol. 27, pp. 1075-1089, 1995.

[21] «Referencia 1,» p. 203.

[22] J. P. M. Trusler et. al, «The Speed of Sound and Derivd Thermodynamics Properties of Methane,»

Journal of Chemical Thermodynamics, vol. 24, pp. 973-991, 1992.

[23] Kunz et al, The GERG-2004 Wide-Range Reference Equation of State for Natural Gases and Other Mixtures, Düsseldorf: Groupe Européen de Recherches Gazières, 2007.

[24] Kunz et al, «The GERG-2008 Wide-Range Equation of State for Natural Gases and Other Mixtures An Expansion of GERG-2004,» *Journal of Chemical & Engineering Data,* vol. 57, pp. 3032-3091, 2012.

[25] Lemmon et al, *NIST Standard Reference Database 23: REFPROP, Version 9.1,* Gaithersburg: NIST Standard Reference Data Program, 2013.

[26] JCGM, «Suplemento 1 de la "Guía para la expresión de la incertidumbre de medida" - Propagación de distribuciones aplicando el método de Monte Carlo,» Centro Español de Metrología, 2010.

[27] R. Hernández-Gómez. et al, «Integration of biogas in the natural gas grid - Thermodynamic characterization of a biogas-like mixture,» *Journal of Chemical Thermodynamics,* vol. 84, pp. 60-66, 2015.